Visibility Aware Human-Object Interaction Tracking from Single RGB Camera

Xianghui Xie   Bharat Lal Bhatnagar   Gerard Pons-Moll

University of Tübingen, Tübingen AI Center, Germany
Max Planck Institute for Informatics, Saarland Informatics Campus, Germany
{xxie, bbhatnag}@mpi-inf.mpg.de, gerard.pons-moll@uni-tuebingen.de

Abstract

Capturing the interactions between humans and their environment in 3D is important for many applications in robotics, graphics, and vision. Recent works to reconstruct the 3D human and object from a single RGB image do not have consistent relative translation across frames because they assume a fixed depth. Moreover, their performance drops significantly when the object is occluded. In this work, we propose a novel method to track the 3D human, object, contacts between them, and their relative translation across frames from a single RGB camera, while being robust to heavy occlusions. Our method is built on two key insights. First, we condition our neural field reconstructions for human and object on per-frame SMPL model estimates obtained by pre-fitting SMPL to a video sequence. This improves neural reconstruction accuracy and produces coherent relative translation across frames. Second, human and object motion from visible frames provides valuable information to infer the occluded object. We propose a novel transformer-based neural network that explicitly uses object visibility and human motion to leverage neighbouring frames to make predictions for the occluded frames. Building on these insights, our method is able to track both human and object robustly even under occlusions. Experiments on two datasets show that our method significantly improves over the state-of-the-art methods. Our code and pretrained models are available at: https://virtualhumans.mpi-inf.mpg.de/VisTracker.

1. Introduction

Perceiving and understanding human as well as their interaction with the surroundings has lots of applications in robotics, gaming, animation and virtual reality etc. Accurate interaction capture is however very hard. Early works employ high-end systems such as dense camera arrays [8, 17, 37] that allow accurate capture but are expensive to deploy. Recent works [6, 34, 36] reduce the require-
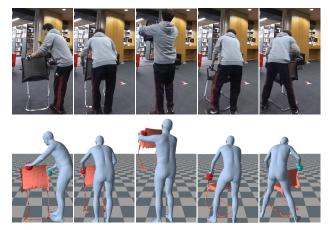

Figure 1. From a monocular RGB video, our method tracks the human, object and contacts between them even under occlusions.

ment to multi-view RGBD cameras but it is still complicated to setup the full capture system hence is not friendly for consumer-level usage. This calls for methods that can capture human-object interaction from a single RGB camera, which is more convenient and user-friendly.

However, reasoning about the 3D human and object from monocular RGB images is very challenging. The lack of depth information makes the predictions susceptible to depth-scale ambiguity, leading to temporally incoherent tracking. Furthermore, the object or human can get heavily occluded, making inference very hard. Prior work PHOSA [91] relies on hand-crafted heuristics to reduce the ambiguity but such heuristic-based method is neither very accurate nor scalable. More recently, CHORE [80] combines neural field reconstructions with model based fitting obtaining promising results. However, CHORE, assumes humans are at a fixed depth from the camera and predicts scale alone, thereby losing the important *relative translation* across frames. Another limitation of CHORE is that it is not robust under occlusions as little information is available from single-frame when the object is barely visible. Hence CHORE often fails in these cases, see Fig. 3.

In this work, we propose the first method that can track

1

both human and object accurately from monocular RGB videos. Our approach combines neural field predictions and model fitting, which has been consistently shown to be more effective than directly regressing pose [4–6, 80]. In contrast to existing neural field based reconstruction methods [61, 80], we can do tracking including inference of relative translation. Instead of assuming a fixed depth, we condition the neural field reconstructions (for object and human) on per frame SMPL estimates (SMPL-T) including translation in camera space obtained by pre-fitting SMPL to the video sequence. This results in coherent translation and improved neural reconstruction. In addition, we argue that during human-object interaction, the object motion is highly correlated with the human motion, which provides us valuable information to recover the object pose even when it is occluded (see Fig. 1 column 3-4). To this end, we propose a novel transformer based network that leverages the human motion and object motion from nearby visible frames to predict the object pose under heavy occlusions.

We evaluate our method on the BEHAVE [6] and InterCap dataset [35]. Experiments show that our method can robustly track human, object and realistic contacts between them even under heavy occlusions and significantly outperforms the currrent state of the art method, CHORE [80]. We further ablate the proposed *SMPL-T conditioning* and *human and visibility aware* object pose prediction network and demonstrate that they are key for accurate human-object interaction tracking.

In summary, our key contributions include:

- We propose the first method that can jointly track full-body human interacting with a movable object from a monocular RGB camera.

- We propose *SMPL-T conditioned interaction fields*, predicted by a neural network that allows consistent 4D tracking of human and object.

- We introduce a novel *human and visibility aware* object pose prediction network along with an object visibility prediction network that can recover object poses even under heavy occlusions.

- Our code and pretrained models are publicly available to foster future research in this direction.

2. Related Work

In this section, we first review recent works that deal with human or object pose estimation and tracking separately. We then discuss recent progresses that model human and object interactions and works that deal with occlusions explicitly.

Human or object pose estimation and tracking. After the introduction of SMPL [49] body model, tremendous progress has been made in human mesh recovery (HMR) from single images [2, 3, 7, 18, 43, 52, 55] or videos [20, 40, 56, 57, 89]. We refer readers to a recent review of HMR methods in [70]. On the other hand, deep learning method has also significantly improved object 6D pose estimation from single RGB images [22, 25, 33, 45, 50, 53, 73]. However, object pose tracking has received less attention and most works focus on RGBD inputs [21, 65, 75, 76, 94]. Two works explore the camera localization ideas from SLAM communities and can track object from RGB videos [48, 68]. Nevertheless, they heavily rely on visual evidence and the performance is unknown under heavy occlusions. They also do not track human-object interactions.

Human-object interaction. Modelling human object interaction is an emerging research topic in recent years. Hand-object interaction is studied with works modelling hand-object interaction from RGB [19, 24, 30, 38, 85], RGBD [9, 11, 28] or 3D inputs [10, 54, 69, 95]. There are also works that model human interacting with a static scene [27, 29, 34, 63, 77, 86, 87] or deformable surface [46]. More recently, the release of BEHAVE [6] and InterCap [35] datasets allows bench-marking of full-body interacting with a movable object. However, human-object interaction capture usually deploys multi-view RGB [67] or RGBD [6, 9, 20, 28, 28, 34, 35, 93] cameras. Only a few works [74, 80, 91] reconstruct dynamic human and object from monocular RGB input and our experiments show that they are not suitable for tracking.

Pose estimation under occlusion. Most existing methods assume occlusion-free input images hence are not robust under occlusions. Only a few methods address human pose estimation under partial occlusions [26, 41, 42, 58, 59, 92] or long term occlusions [89]. For object pose estimation, pixel-wise voting [53] and self-occlusion [22] are explored for more robust prediction under occlusions. More recently, TP-AE [94] predicts object occlusion ratio to guide pose estimation but relies on depth input. Although being impressive on separate human or object pose estimation, these methods do not reason about human-object interaction. Our method is the first one that takes both human and object visibility into account for interaction tracking.

3. Method

We present a novel method for jointly tracking the human, the object and the contacts between them, in 3D, from a monocular RGB video. The first main challenge in monocular tracking is the estimation of human and object translations in camera space due to the depth-scale ambiguity problem. Existing method, CHORE [80], reconstructs human and object at a fixed depth to the camera, leading to inconsistent 3D translation across frames. Our key idea is to fit a SMPL model with single shape parameters to a video sequence to obtain consistent relative translation across frames. We call the estimated SMPL as SMPL-T
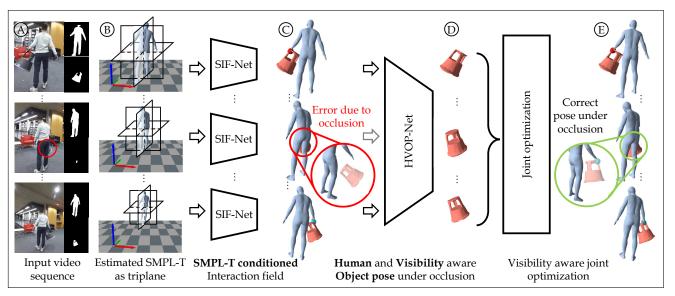
Figure 2. Given an input RGB sequence of a human interacting with an object and their corresponding human-object masks (A), we aim to reconstruct and track the 3D human, object and the contacts between them (E). Our first key idea is a SMPL-T conditioned interaction field network (SIF-Net, details in Sec. 3.3) that predicts neural fields conditioned on estimated SMPL meshes in camera space (col. B, SMPL-T, details in Sec. 3.2). SMPL-T conditioning provides us temporally consistent relative translation, which is important for coherent 4D tracking. Our second key insight is to predict object pose under occlusions (D) leveraging human motion and object visibility information (HVOP-Net, details in Sec. 3.4). This prediction provides robust object tracking for frames with heavy occlusion. We then jointly optimize human and object (details in Sec. 3.5) to satisfy image observations and contact constraints.

and describe it in more details in Sec. 3.2. Based on the estimated SMPL-T, we then jointly model the 3D human, object and the interactions using our proposed *SMPL-T conditioned Interaction Fields* network (SIF-Net, Sec. 3.3)

Object tracking from a single-frame only, is difficult when the object is barely visible. Hence we introduce a *Human and Visibility aware Object Pose Network* (HVOP-Net) that leverages human and object motion from visible frames to recover the object under occlusion (Sec. 3.4). We then use the SIF-Net and HVOP-Net outputs to optimize SMPL model and object pose parameters of this sequence to satisfy neural prediction and image observations (Sec. 3.5). An overview of our approach can be found in Fig. 2.

3.1. Preliminaries

In this work, we focus on a single human interacting with an object, which is a common setting in other hand-object interaction [69, 85, 95] and full body-object interaction works [6, 35, 80]. We represent human using the SMPL [49] body model $H(\theta, \beta)$ that parameterises the 3D human mesh using pose θ (including global translation) and shape β parameters. The object is represented by a known mesh template and we estimate the rotation $\mathbf{R}^o \in SO(3)$ and translation $\mathbf{t}^o \in \mathbb{R}^3$ parameters. Given a video sequence $\{\mathbf{I}_1, ..., \mathbf{I}_T\}$ where $\mathbf{I}_i \in \mathbb{R}^{H \times W \times 5}$ (RGB, human and object masks), our goal is to estimate the SMPL shape β, a sequence of SMPL pose $\mathbf{\Theta} = \{\theta_1, ..., \theta_T\}$, object rota-

tion $\mathcal{R}^o = \{\mathbf{R}_1^o, ..., \mathbf{R}_T^o\}$ and translation $\mathcal{T}^o = \{\mathbf{t}_1^o, ..., \mathbf{t}_T^o\}$ parameters that satisfy 2D image observation and realistic interaction constraints between the human and the object.

3.2. SMPL-T: Temporally consistent SMPL meshes in camera space

Our first step is to obtain SMPL meshes in camera space that have consistent translation in a video sequence. We leverage 2D body keypoint predictions from openpose [12] and natural motion smoothness for this. Specifically, we use FrankMocap [60] to initialise SMPL-T pose $\mathbf{\Theta} = \{\theta_1, ..., \theta_T\}$ and shape $\mathcal{B} = \{\beta_1, ..., \beta_T\}$ parameters for a sequence of images. Note here the original SMPL meshes from FrankMocap are centered at origin. We average the SMPL-T shape parameters over the sequence as the shape for the person and optimize the SMPL-T global translation and body poses to minimize 2D reprojection and temporal smoothness error:

$$E(\mathbf{\Theta}) = \lambda_{\text{J2D}} L_{\text{J2D}} + \lambda_{\text{reg}} L_{\text{reg}} + \lambda_a L_{\text{accel}} + \lambda_{\text{pi}} L_{\text{pi}} \quad (1)$$

where L_{J2D} is the sum of body keypoint reprojection losses [7] over all frames and L_{reg} is a regularization on body poses using priors learned from data [49, 52, 71]. L_{accel} is a temporal smoothness term that penalizes large accelerations over SMPL-T vertices H_i: $L_{\text{accel}} = \sum_{i=0}^{T-2} \|H_i - 2H_{i+1} + H_{i+2}\|_2^2$. L_{pi}, an L2 loss between optimized and initial body

pose, prevents the pose from deviating too much from initialization. λ_* denotes the loss weights detailed in Supp.

Note that this optimization does not guarantee that we get the absolute translation in the world coordinates, it just ensures that our predictions will be consistent with the SMPL model over a sequence, i.e. we will be off by one rigid transformation for the entire sequence.

3.3. SIF-Net: SMPL-T conditioned interaction field

Our SMPL-T provides translation about the human but does not reason about the object and the interaction between them. Existing method CHORE [80] can jointly reason human and object but their humans are predicted at fixed depth. Our key idea is to leverage our SMPL-T meshes to jointly reason human, object and interaction while having consistent relative translation. We model this using a single neural network which we call SIF-Net. The input to SIF-Net consists of RGB image, human and object masks, and our estimated SMPL-T. With features from SMPL-T and input images, it then predicts interaction field which consists of human and object distance fields, SMPL part correspondence field, object pose and visibility field.

SIF-Net feature encoding. Existing neural implicit methods [61, 62, 80] rely mainly on features from input image, a main reason that limits their human prediction at fixed depth. Instead, we extract features from both our estimated SMPL-T meshes and input image, providing more distinct features for the query points along the same ray. Inspired by EG3D [13], we use the triplane representation for SMPL-T feature learning due to its efficiency. Specifically, we use orthographic camera $\pi^o(\cdot)$, to render the SMPL-T mesh silhouette from right, back and top-down views and obtain three images $\mathbf{S}_i^r, \mathbf{S}_i^b, \mathbf{S}_i^t$ respectively, where $\mathbf{S}^i \in \mathbb{R}^{H \times W}$, see supplementary for more visualization. Note here the triplane origin is placed at our SMPL-T mesh center (Fig. 2 B). We then train an image encoder $f^{\text{tri}}(\cdot)$ that extracts a pixel aligned feature grid $\mathbf{D}_i^j \in \mathbb{R}^{H_c \times W_c \times C}$ from each rendered view $\mathbf{S}_i^j$, where $j \in \{r, b, t\}$ and H_c, W_c, C are the feature grid dimensions. To extract features for a query point $\mathbf{p} \in \mathbb{R}^3$, we project $\mathbf{p}$ into the three planes using the same orthographic projection $\pi_{\mathbf{p}}^o = \pi^o(\mathbf{p})$ and extract local features $\mathbf{D}_i^{\mathbf{P}} = (\mathbf{D}_i^r(\pi_{\mathbf{p}}^o), \mathbf{D}_i^b(\pi_{\mathbf{p}}^o), \mathbf{D}_i^t(\pi_{\mathbf{p}}^o))$ using bilinear interpolation.

In addition to the SMPL-T features, SIF-Net also extracts information from input images. More specifically, we train an image encoder $f^{\text{enc}}(\cdot)$ to extract feature grid $\mathbf{Z}_i \in \mathbb{R}^{H_f \times W_f \times C_f}$ from input image $\mathbf{I}_i \in \mathbb{R}^{H \times W \times 5}$, here H_f, W_f, C_f and H, W are feature grid and input image dimensions respectively. Given query point $\mathbf{p} \in \mathbb{R}^3$, we project it to 2D image using full perspective projection $\pi_{\mathbf{p}} = \pi(\mathbf{p})$ and extract pixel-aligned features $\mathbf{Z}_i^{\mathbf{P}} = \mathbf{Z}_i(\pi_{\mathbf{p}})$. The input image feature is concatenated with the SMPL-T feature to form an input and translation aware

point feature: $\mathbf{F}_i^{\mathbf{P}} = (\mathbf{Z}_i^{\mathbf{P}}, \mathbf{D}_i^{\mathbf{P}})$.

SIF-Net predictions. From the point feature $\mathbf{F}_i^{\mathbf{P}}$ discussed above, we predict our interaction fields that jointly model human, object and their contacts, similar to CHORE [80]. Specifically, we predict the unsigned distances to human and object surfaces using $f^u : \mathbf{F}_i^{\mathbf{P}} \mapsto \mathbb{R}_{\geq 0}^2$. This allows fitting the SMPL mesh and object template by minimizing the predicted distances at mesh vertices. We can also infer contacts, as the points having small distances to both human and object surfaces. For more robust SMPL fitting [4] and modelling which body part the object point is in contact with, we predict SMPL part correspondence using $f^p : \mathbf{F}_i^{\mathbf{P}} \mapsto \{1, 2, ..., K\}$ where K is the number of SMPL parts. For more accurate object fitting, we additionally predict object rotation with $f^R : \mathbf{F}_i^{\mathbf{P}} \mapsto \mathbb{R}^{3 \times 3}$ and translation with $f^c : \mathbf{F}_i^{\mathbf{P}} \mapsto \mathbb{R}^3$. The predicted 3×3 matrix is projected to SO(3) using symmetric orthogonalization [44]. At test time, we first use f^u to find points on the object surface [16] and take the average rotation and translation predictions of these points as the object pose. To handle occlusions, we also predict the object visibility field using $f^{\text{vis}} : \mathbf{F}_i^{\mathbf{P}} \mapsto [0, 1]$. The visibility is useful to recover the object pose under occlusion, see more details in Sec. 3.4.

Why use triplane to encode SMPL-T? A direct alternative to triplane based SMPL-T encoding is to find the closest point in SMPL-T mesh and concatenate that coordinate to the point features. But such a method is slow (computing point to surface distance) and does not allow flexible learning of local and global features. Another choice is to voxelize the SMPL-T mesh and extract point local features using IF-Nets [15] but such a method is still expensive. Therefore we chose the more efficient triplane representation to encode our estimated SMPL-T meshes.

Implementation. Our SMPL-T feature extractor f^{tri} is shared for three views and trained end to end with image encoder f^{enc} and other neural field predictors. At training time, we input the renderings from ground truth SMPL meshes and train the network to predict GT labels. At test time, we obtain the SMPL-T meshes using Eq. (1). In order to have smoother SMPL-T feature in a sequence, we use SmoothNet [90] to smooth the optimized SMPL parameters. We evaluate this component and provide more implementation details in supplementary.

3.4. HVOP-Net: Human and Visibility aware Object Pose under occlusions

Our SIF-Net recovers translation and more accurate object pose. However, the object pose prediction under very heavy occlusions remains challenging because no image evidence from single frame is available for accurate prediction, see Fig. 5. Our key idea is to use the SMPL-T and object pose from other visible frames to predict the object of occluded frames. To this end, we first predict object vis-

ibility scores in each image, which are then leveraged together with the human evidence from neighbouring frames to predict the object poses of the occluded frames.

Object visibility score. Our visibility score denotes how much the object is visible in the input image. We train a visibility decoder $f^{\text{vis}}(\cdot)$, a prediction head of SIF-Net, that takes a point feature $\mathbf{F}_i^{\mathbf{P}}$ as input and predicts visibility score $v_i \in [0, 1]$ for frame i. At test time, we first use the neural object distance predictor f^u to find object surface points [16] and then take the average visibility predictions of these points as the object visibility score for this image.

Object pose prediction under heavy occlusion. Our goal now is to predict accurate object pose for heavily occluded frames. We consider frames whose visibility score v_i is smaller than $\delta = 0.5$ as the occluded frames. Inspired by works from motion infill [23,39] and synthesis [88,93], we design our HVOP-Net that leverages transformer [72] and explicitly takes the human motion and object visibility into account to recover object pose under heavy occlusions.

More specifically, we first use a transformer $f^s(\cdot)$ to aggregate temporal information of the SMPL-T poses: $f^s : \mathbb{R}^{T \times |\theta_i|} \mapsto \mathbb{R}^{T \times D_{hs}}$, where $|\theta_i|$ is the SMPL pose dimension and D_{hs} is the hidden feature dimension. Similarly, we use a transformer $f^o(\cdot)$ to aggregate temporal information of the object poses: $f^o : \mathbb{R}^{T \times D_o} \mapsto \mathbb{R}^{T \times D_{ho}}$. Note here the SMPL-T transformer f^s attends to all frames while the object transformer f^o only attends to frames where object is visible ($v_i \geq \delta$). We then concatenate the SMPL-T and object features and use another transformer f^{comb} to aggregate both human and object information and predict the object poses: $f^{\text{comb}} : \mathbb{R}^{T \times (D_{hs} + D_{ho})} \mapsto \mathbb{R}^{T \times D_o}$. The joint transformer f^{comb} attends to all frames. Our experiments show that our HVOP-Net is important to accurately predict object pose under heavy occlusions, see Fig. 5.

Implementation. The visibility decoder f^{vis} is trained end to end with other SIF-Net components using L2 loss. The GT visibility score is computed as the number of visible object pixels (from object mask) divided by total number of object pixels (from GT object rendering). To train our HVOP-Net, we randomly zero out the object pose for a small clip of the input sequence and provide ground truth SMPL and object poses for other frames as input. We train our network to accept input sequence of a fixed length but at test time, the sequence can have various length and object occlusion can last for a longer time. To this end, we use an auto-regressive algorithm to recover the object pose of a full video, similar to [89]. At test time, we use SIF-Net object pose predictions and zero out highly occluded frames based on the predicted visibility scores. We empirically find that having smooth object pose as input is helpful for more accurate prediction. Hence we use SmoothNet [90] to smooth SIF-Net object pose predictions before inputing them to HVOP-Net. The evaluation of this component and

more training details are described in our supplementary.

3.5. Visibility aware joint optimization

To obtain SMPL and object meshes that align with input images and satisfy contact constraints, we leverage our network predictions from Sec. 3.3 and Sec. 3.4 to formulate a robust joint optimization objective. Our goal is to obtain an optimal set of parameters $\mathbf{\Phi} = \{\mathbf{\Theta}, \boldsymbol{\beta}, \mathcal{R}^o, \mathcal{T}^o\}$ for SMPL pose, shape, object rotation and translation respectively. We initialize the SMPL parameters from our estimated SMPL-T (Eq. (1)) and object parameters from our HVOP-Net predictions (Sec. 3.4). Inspired by CHORE [80], our energy function consists of human data E_{data}^h, object data E_{data}^o, contact data E_{data}^c and SMPL pose prior term E_{reg}:

$$E(\mathbf{\Phi}) = E_{data}^h + E_{data}^o + E_{data}^c + E_{reg}. \quad (2)$$

here E_{reg} is a body pose and shape prior loss [49]. We explain other loss data terms next.

Human data term. E_{data}^h minimizes the discrepancy between SIF-Net prediction and SMPL meshes as well as a temporal smoothness error: $E_{data}^h(\mathbf{\Theta}, \boldsymbol{\beta}) = \sum_{i=1}^{T} L_{\text{neural}}^h(\boldsymbol{\theta}_i, \boldsymbol{\beta}) + \lambda_{\text{ah}} L_{\text{accel}}(\mathbf{\Theta})$, where L_{accel} is the same used in Eq. (1). L_{neural}^h pushes the SMPL vertices to the zero-level set of the human distance field represented by neural predictor $f_i^{u,h}$ and forces correct SMPL part locations predicted by f_i^p:

$$E_{\text{neural}}^h(\mathbf{\Theta}, \boldsymbol{\beta}) = \sum_{i=1}^{T} \Big(\sum_{\mathbf{p} \in H(\boldsymbol{\theta}_i, \boldsymbol{\beta})} (\lambda_h \min(f_i^{u,h}(\mathbf{F}_i^{\mathbf{P}}), \delta_h) + \lambda_p L_p(l_{\mathbf{p}}, f_i^p(\mathbf{F}_i^{\mathbf{P}}))) \Big) \quad (3)$$

here $l_{\mathbf{p}}$ is the predefined SMPL part label [4] of SMPL vertex $\mathbf{p}$ and L_p is the categorical cross entropy loss function. δ_h is a small clamping value.

Object data term. We transform the object template vertices $\mathbf{O} \in \mathbb{R}^{3 \times N}$ using object pose parameters of frame i by: $\mathbf{O}_i' = \mathbf{R}_i^o \mathbf{O} + \mathbf{t}_i^o$. Intuitively, the object vertices should lie on the zero-level set of the object distance field represented by $f_i^{u,o}$ and the rendered silhouette should match the 2D object mask $\mathbf{M}_i^o$. Hence we formulate the loss as:

$$E_{data}^o(\mathcal{R}^o, \mathcal{T}^o) = \sum_{i=1}^{T} v_i \Big(\sum_{\mathbf{p} \in \mathbf{O}_i'} \lambda_o \min(f_i^{u,o}(\mathbf{F}_i^{\mathbf{P}}), \delta_o) + \lambda_{\text{occ}} L_{\text{occ-sil}}(\mathbf{O}_i', \mathbf{M}_i^o) \Big) + \lambda_{\text{ao}} L_{\text{ao}} \quad (4)$$

where v_i is the predicted object visibility score described in Sec. 3.4. This down-weights the loss values of network predictions for frames where object is occluded and allows more temporal regularization. $L_{\text{occ-sil}}$ is an occlusion-aware silhouette loss [91] and L_{ao} is a temporal smoothness loss applied to object vertices $\mathbf{O}_i'$, similar to L_{accel} in Eq. (1).

Contact data term. The contact data term [80] minimizes the distance between human and object points that are predicted to be in contact:

$$E_{\text{data}}^c(\mathcal{R}^o, \mathcal{T}^o) = \lambda_c \sum_{i=1}^{T} (\sum_{j=1}^{K} d(H_j^c(\boldsymbol{\theta}_i, \boldsymbol{\beta}), \mathbf{O}_{ij}^c)) \quad (5)$$

here $d(\cdot, \cdot)$ is chamfer distance. We consider human points on the jth body part of SMPL mesh H_i of frame i (denoted as H_{ij}) are in contact when their predicted distance to the object is smaller than a threshold: $H_j^c(\boldsymbol{\theta}_i, \boldsymbol{\beta}) = \{\mathbf{p}|\mathbf{p} \in H_{ij}$ and $f_i^{u,o}(\mathbf{F}_i^\mathbf{P}) \leq \epsilon\}$. Similarly, we find contact points on object meshes with $\mathbf{O}_{ij}^c = \{\mathbf{p}|\mathbf{p} \in \mathbf{O}_i'$ and $f_i^{u,h}(\mathbf{F}_i^\mathbf{P}) \leq \epsilon$ and $f_i^p(\mathbf{F}_i^\mathbf{P}) = j\}$.

Please see Supp. for more details about loss weights λ_*.

4. Experiments

In this section, we first compare our method against existing approaches on tracking human and object and then evaluate the key components of our methods. Our experiments show that our method clearly outperforms existing joint human object reconstruction method and our novel *SMPL-T conditioned interaction fields* (SIF-Net) as well as *human and visibility aware* object pose prediction (HVOP-Net) works better than existing state of the art methods.

Baselines. (1) Joint human and object tracking. We compare against PHOSA [91] and CHORE [80] in the joint human-object reconstruction task. **(2) Object pose prediction.** Our HVOP-Net leverages nearby (un-occluded) frames to predict the object pose of occluded frames. We compare this with a simple baseline that linearly interpolates the object pose between visible frames to recover occluded poses. We also find similarity between our task and motion smoothing/infilling. Hence we compare our HVOP-Net with SoTA smoothing [90] and infill method [39].

Datasets. We conduct experiments on the BEHAVE [6] and InterCap [35] dataset. **(1) BEHAVE** [6] captures 7 subjects interacting with 20 different objects in natural environments and contains SMPL and object registrations annotated at 1fps. We use the extended BEHAVE dataset, which registers SMPL and object for BEHAVE sequences at 30 fps. We follow the official split [80] with 217 sequences for training and 82 for testing. **(2) InterCap** [35] is a similar dataset that captures 10 subjects interacting with 10 different objects. The dataset comes with pseudo ground truth SMPL and object registrations at 30fps. We train our model on sequences from subject 01-08 (173 sequences) and test on sequences from subject 09-10 (38 sequences).

We compare with CHORE [80] on the full test set of both datasets. PHOSA [91] optimizes hundreds of random object pose initialization per image hence the inference speed is very slow (2min/image), which makes it infeasible to run on full video sequences. Hence we compare with PHOSA

on key frames only, denoted as BEHAVE*(3.9k images) and InterCap*(1.1k images) respectively. Due to the large number of frames in the full BEHAVE test set (127k frames), we conduct other ablation experiments in a sub test set (42k frames) of BEHAVE.

Evaluation metrics. (1) Joint human-object tracking. We evaluate the performance of SMPL and object reconstruction using Chamfer distance between predicted SMPL and object meshes, and the ground truth. CHORE [80] uses Procrustes alignment on combined SMPL and object meshes for *each frame* before computing errors. However, this does not reflect the real accuracy in terms of the relative translation between nearby frames in a video. Inspired by the world space errors proposed by SPEC [42] and GLAMR [89], we propose to perform joint Procrustes alignment in a sliding window, as also used in SLAM evaluations [31, 66]. More specifically, we combine all SMPL and object vertices within a sliding window and compute a single optimal Procrustes alignment to the ground truth vertices. This alignment is then applied to all SMPL and object vertices within this window and Chamfer distance of SMPL and object meshes are computed respectively. We report both the errors using per-frame alignment (w=1) and alignment with a sliding window of 10s (w=10).
(2) **Object only evaluation.** For experiments evaluating object pose only, we evaluate the rotation accuracy using rotation angle [32]. The object translation error is computed as the distance between reconstructed and GT translation. We report all errors in centimetre in our experiments.

4.1. Evaluation of tracking results

Dateset	Methods	Align w=1		Align w=10	
		SMPL ↓	Obj. ↓	SMPL ↓	Obj. ↓
BEHAVE	CHORE	5.55	10.02	18.33	20.32
	Ours	**5.25**	**8.04**	**7.81**	**8.49**
BEHAVE*	PHOSA	12.86	26.90	27.01	59.08
	CHORE	5.54	10.12	21.28	22.39
	Ours	**5.24**	**7.89**	**8.24**	**8.49**
InterCap	CHORE	7.12	12.59	16.11	21.05
	Ours	**6.76**	**10.32**	**9.35**	**11.38**
InterCap*	PHOSA	11.20	20.57	24.16	43.06
	CHORE	7.01	12.81	16.10	21.08
	Ours	**6.78**	**10.34**	**9.35**	**11.54**

Table 1. Human and object tracking results on BEHAVE [6] and InterCap [35] datasets (unit: cm). * denotes key frames only. w is the temporal window size used for Procrustes alignment where w=1 means per-frame Procrustes and w=10 means alignment over a sliding window of 10s. We can see our method clearly outperforms baseline PHOSA [91] and CHORE [80] in all metrics.

We compare our human and object tracking results against baseline PHOSA [91] and CHORE [80] and report the errors in Tab. 1. Note that the comparison with PHOSA

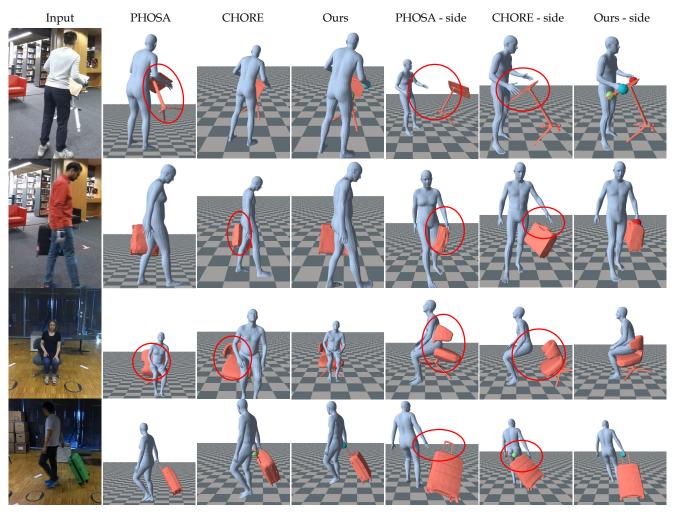| Input | PHOSA | CHORE | Ours | PHOSA - side | CHORE - side | Ours - side |

Figure 3. Comparison with PHOSA [91] and CHORE [80] on BEHAVE [6] (row 1-2) and InterCap [35] (row 3-4). PHOSA's object pose optimization often gets stuck in local minima due to heavy occlusions. CHORE also fails to predict accurate object pose as it does not fully explore the human, temporal and visibility information while our method can robustly track human and object in these challenging cases.

and CHORE is not strictly fair as they do not use temporal information. Nevertheless they are our closest baselines and we show that our method outperforms them using per-frame alignment and is significantly better under a more relevant evaluation metric (align w=10) for video tracking. We also show qualitative comparisons in Fig. 3. It can be seen that both PHOSA and CHORE are not able to accurately capture the object under heavy occlusions while our method is more robust under these challenging occlusion cases.

4.2. Importance of SMPL-T conditioning

We propose to condition our interaction field predictions on SMPL-T meshes, we evaluate this for the joint tracking task in Tab. 2. Our SMPL-T conditioning allows us to obtain consistent relative translation instead of predicting the human at fixed depth. This significantly reduces the error when evaluating using alignment of temporal sliding win-

Method	w/o SMPL-T	w/o HVOP-Net	w/o joint opt.	**Ours**
SMPL ↓	14.40	8.05	8.20	**8.03**
Obj. ↓	17.29	9.36	16.02	**8.23**

Table 2. Ablation studies. We report the joint tracking error (cm) after an alignment window of 10s. It can be seen that our proposed SMPL-T conditioning, HVOP-Net and joint optimization are important to achieve the best results.

dow, see Tab. 2 and qualitative examples in Supp.

Note that the SIF-Net prediction relies on the estimated SMPL-T discussed in Sec. 3.2. We also evaluate how the noisy SMPL-T predictions can affect the joint tracking performance. We input GT SMPL to our SIF-Net and HVOP-Net to predict the object pose and perform joint optimization. The object errors (Chamfer distance in cm) are: 17.29 (w/o SMPL-T cond.), 8.23 (w/ SMPL-T cond., ours), 6.50 (GT SMPL). Our method is robust and is close to the ideal lower bound with GT SMPL.
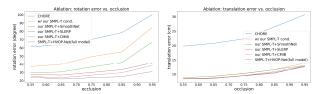
Figure 4. Object rotation(left) and translation(right) error vs. occlusion (1-fully occluded) for variants of our method. Our full model with HVOP-Net predicts more robust rotation in occlusions.
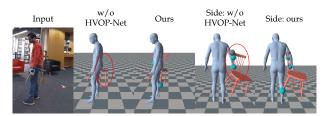

Figure 5. Importance of our HVOP-Net object pose prediction. We can see that our HVOP-Net corrects erroneous object pose under heavy occlusions. Better viewed after zoom in.

4.3. Importance of HVOP-Net

We propose a *human and visibility aware* object pose prediction network (HVOP-Net) to reason about the object under heavy occlusions. Without this component, the object error is much higher (Tab. 2 column 3), which suggests the importance of our HVOP-Net.

For the object pose prediction task, there are other similar alternatives to HVOP-Net: 1). Linear interpolation (SLERP), infill the object pose of invisible frames using spherical linear interpolation between two visible frames. 2). SmoothNet [90], a fully connected neural network trained to smooth the object motion. 3). CMIB [39], a SoTA method for human motion infilling. To evaluate the effectiveness of our HVOP-Net, we replace HVOP-Net with these methods and run the full tracking pipeline respectively. The SMPL errors are similar (deviate < 0.1cm) as HVOP-Net only affects objects. We separate object error into rotation (angle distance) and translation, and further analyse the error under varying occlusion for CHORE, our method (SMPL-T + HVOP-Net) and its variants (SMPL-T + SmoothNet/SLERP/CMIB) in Fig. 4.

All methods except CHORE predict similar translation (due to SMPL-T cond.) but our HVOP-Net obtains clearly more robust rotation under heavy occlusions. SmoothNet smooths the object motion but cannot correct errors from long-term occlusions. SLERP and CMIB [39] are able to correct some pose errors but do not take the human context into account hence cannot handle heavy occlusions very well. Our method leverages the human motion and object pose from visible frames hence achieves the best result. We show one example where our HVOP-Net corrects the erroneous raw prediction in Fig. 5. Please see our supplementary for more examples.

Figure 6. Results in NTU-RGBD dataset [47]. It can be seen that our method generalizes well and wormks better than CHORE [80].

4.4. Generalization

To verify the generalization ability of our method, we apply our model trained on BEHAVE to the NTU-RGBD [47] dataset. We leverage Detectron [79], interactive [64] and video [14] segmentation to obtain the input human and object masks. Two example comparisons with CHORE [80] are shown in Fig. 6. We can see our method generalizes well to NTU-RGBD and works better than CHORE. Please see Supp. for evaluation details and more comparisons.

5. Limitations

Although our method works robustly under heavy occlusions, there are still some limitations. For instance, we assume known object templates for tracking. An interesting direction is to build such a template from videos as demonstrated by recent works [78,82–84]. Our method may fail under challenging cases such as significant object pose change under heavy occlusions. It can also make noisy pose predictions when the object is symmetric or the pose is uncommon. Example failure cases are shown in Supp.

6. Conclusion

We present a novel method for tracking human, object and realistic contacts between them from monocular RGB cameras. Our first contribution is a SMPL-T conditioned neural field network that allows consistent and more accurate 3D reconstruction in a video sequence. Our second contribution is a human motion and object visibility aware network that can recover the object pose under heavy occlusions. Our experiments show that our method significantly outperforms state of the art methods in two datasets. Our extensive ablations show that our SMPL-T conditioning and HVOP-Net are important for accurate tracking. We also show that our method generalizes well to another dataset it is not trained on. Our code and model are released to promote future research in this direction.

Appendices

In this supplementary, we first list all the implementation details of our method and then show more ablation study results as well as comparison with CHORE [80] on NTU-RGBD [47] dataset. We end with discussions of failure cases and future works.

Appendix A. Implementation details

A.1. Obtaining SMPL-T meshes

To obtain the image-aligned SMPL meshes that have consistent translation (SMPL-T) we keep the SMPL shape parameters and optimize the body pose and global translation values. The loss weights for this optimization are: $\lambda_{\text{J2D}} = 0.09, \lambda_{\text{reg}} = 1.0 \times 10^{-5}, \lambda_a = 25, \lambda_{\text{pi}} = 900$. We optimize the parameters until convergence with a maximum iteration of 1000.

A.2. SIF-Net: SMPL-T conditioned interaction field

A visualization of our SMPL-T triplane rendering and query point projection can be found in Fig. 7. We discuss our network architecture and training details next.

Network architecture. We use the stacked hourglass network [51] for both RGB image encoder f^{enc} and SMPL rendering encoder f^{tri}. We use 3 stacks for f^{tri} and the output feature dimension is $d_o^{\text{tri}} = 64$. Hence $f^{\text{tri}} : \mathbb{R}^{H \times W} \mapsto \mathbb{R}^{H/4 \times W/4 \times 64}$ where $H = W = 512$. We also use 3 stacks for f^{enc} but the feature dimension is $d_o^{\text{enc}} = 256$. Hence $f^{\text{enc}} : \mathbb{R}^{H \times W \times 5} \mapsto \mathbb{R}^{H/4 \times W/4 \times 256}$. We also concatenate the image features extracted from the first convolution layer and query point coordinate to the features. Thus the total feature dimension to our decoders is: $d = (d_1^{\text{tri}} + d_o^{\text{tri}}) \times 3 + d_1^{\text{enc}} + d_o^{\text{enc}} + 3 = 611$, here $d_1^{\text{tri}} = 32, d_1^{\text{enc}} = 64$. All decoders consist of three FC layers with ReLU activation and one output FC layer with hidden dimension of 128 for the intermediate features. The visibility decoder f^v additionally has a sigmoid output activation layer. The output shape is $2, 14, 9, 3, 1$ for f^u, f^p, f^R, f^c, f^v respectively.

Training. All feature encoders and decoders are trained end to end with the loss: $L = \lambda_u(L_{u_h} + L_{u_o}) + \lambda_p L_p + \lambda_R L_R + \lambda_c L_c + \lambda_v L_v$. Here L_{u_i} is the L_1 distance between ground truth and predicted unsigned distance to human or object surface [80]. L_p is a standard categorical

A. right   B. back   C. top-down

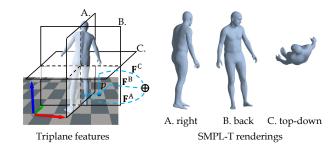Triplane features   SMPL-T renderings

Figure 7. Visualization of our SMPL-T triplane feature extraction and rendering. The triplane origin is placed at the SMPL-T body center and we render the mesh from three views using orthographic projection: righ-left (A), back-front (B) and top-down (C). The query point p is projected into the three planes using same projection for rendering and we extract pixel aligned features $\mathbf{F}^A, \mathbf{F}^B, \mathbf{F}^C$ from the feature planes respectively. Note that we render the SMPL-T with color here for visualization, the actual input to our network are silhouette images only.

cross entropy loss for SMPL part correspondence prediction. L_R, L_c, L_v are mean square losses between ground truth and predicted values for rotation matrix, translation vector and visibility score respectively. The loss weights are: $\lambda_u = 1.0, \lambda_R = 0.006, \lambda_c = 500, \lambda_c = \lambda_v = 1000$. The model is trained for 18 epochs and it takes 25h to converge on a machine with 4 RTX8000 GPUs each with 48GB memory. The training batch size is 8.

A.3. HVOP-Net: object pose under occlusion

We use three transformers $f^s, f^o, f^{\text{comb}}$ to aggregate features from SMPL-T, object pose and joint human object information respectively. We use the 6D vector [96] to represent the ration matrix of SMPL-T and object pose parameters. Hence the SMPL-T pose dimension is $24 \times 6 + 3 = 147$, where 3 denotes the global translation. We predict the object rotation only thus the object data dimension is 6. The SMPL-T transformer f^s consists of an MLP: $\mathbb{R}^{T \times 147} \mapsto \mathbb{R}^{T \times 128}$ and two layers of multi-head self-attention (MHSA) module [72] with 4 heads. Similarly, the object transformer f^o consists of an MLP: $\mathbb{R}^{T \times 6} \mapsto \mathbb{R}^{T \times 32}$ and two layers of MHSA module with 2 heads. The joint transformer f^{comb} consists of 4 layers of MHSA module with 1 head only. GeLU activation is used in all MHSA modules. We finally predict the object pose using two MLP layers with an intermediate feature dimension of 32 and LeakyReLU activation.

The model is trained to minimize the L_1 losses of pose value and accelerations: $L = \lambda_{\text{pose}} L_{\text{pose}} + \lambda_{\text{accel}} L_{\text{accel}}$, where $\lambda_{\text{pose}} = 1.0, \lambda_{\text{accel}} = 0.1$. It is trained on a server with 2 RTX8000 GPUs, each GPU has 48GB memory capacity. It takes around 7h to converge (64 epochs).

9

A.4. SmoothNet for SMPL-T and object

We use SmoothNet [90] to smooth our SMPL-T and SIF-Net object pose predictions. We use exactly the same model and training strategy proposed by the original paper. The input to the SMPL-T SmoothNet is our estimated SMPL-T pose and translation (relative to the first frame). The input to the object SmoothNet is the object rotation (6D vector). Following the standard practice of SmoothNet [90], we train both models on the predictions from the BEHAVE [6] training set. Note that we do not fine-tune them on InterCap [35] dataset. We evaluate this component in Sec. B.3.

A.5. Visibility aware joint optimization

The objective function defined in Eq. 2 is highly non-convex thus we solve this optimization problem in two stages. We first optimize the SMPL pose and shape parameters using human data term only. We then optimize the object parameters using the object and contact data terms. The loss weights are set to: $\lambda_{reg} = 2.5 \times 10^{-4}$, $\lambda_{ah} = 10^4$, $\lambda_h = 10^4$, $\lambda_p = t \times 10^{-4}$, $\lambda_o = 900$, $\lambda_{occ} = 9 \times 10^{-4}$, $\lambda_{ao} = 225$, $\lambda_c = 900$, where λ_c is the loss weight for the contact data term defined in Eq. 5.

Appendix B. Additional ablation results

B.1. Further evaluation of SMPL-T conditioning

We show some example images from one sequence in Fig. 8 to evaluate the importance of our SMPL-T conditioning. It can be seen that without this conditioning, the human is reconstructed at fixed depth, leading to inconsistent relative translation across time. Our method predicts more coherent relative human translation and more accurate object pose.

To further evaluate SMPL-T conditioning, we compute the object pose error from the raw network predictions and compare it with the object pose of CHORE which is also the raw prediction from the network. The pose error is computed as Chamfer distance (CD) and vertex to vertex (v2v) error after centring the prediction and GT mesh at origin. We also report the translation error (transl.) as the distance between predicted and GT translation. The results are shown in Tab. 3. We can clearly see that our SMPL feature improves both the raw object pose prediction and distance fields (results after optimization are also improved).

B.2. Comparing different pose prediction methods

We show some example comparisons of different object pose prediction methods under heavy occlusions in Fig. 10. We compare our method against: 1). Raw prediction from our SIF-Net. 2). Linearly interpolate the occluded poses from visible frames (SLERP). 3). CMIB [39], a transformer based model trained to infill the object motion using visible

| Method | Raw prediction | | | After opt. w=10 | |
	CD↓	v2v↓	transl.↓	SMPL↓	obj.↓
w/o SMPL-T	5.56	16.10	14.28	14.40	17.29
Ours	**3.98**	**12.34**	**9.53**	**8.03**	**8.23**

Table 3. Importance of SMPL-T conditioning (errors in cm). We can see that our SMPL-T feature improves both the raw object pose prediction and distance fields (after opt.). Without our SMPL-T conditioning, the reconstructed translation is not consistent across frames, leading to large errors after alignment of temporal window of 10s (w=10).
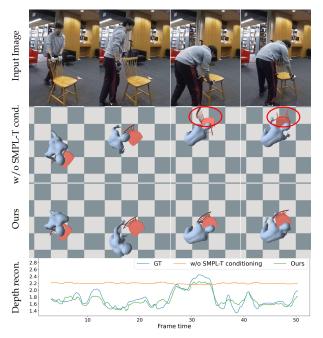

Figure 8. Evaluating SMPL-T conditioning for neural field prediction. We can see that without conditioning on SMPL-T meshes, the object pose prediction is worse and human is reconstructed at fixed depth, leading to inconsistent relative location across frames. Our method recovers the relative translation more faithfully and obtain better object pose predictions.

frames. Note here the evaluation is based on the final tracking results and we report the object errors only as the difference of SMPL error is very small. Similar to Sec. B.1, the object errors are computed as Chamfer distance, v2v error and translation error.

It can be seen that the raw pose prediction is noisy due to occlusion. SLERP and CMIB corrects some pose errors but is not robust as they do not leverage the human information. Our method is more accurate as it takes the human context and object pose into account.

B.3. Evaluating SmoothNet

SmoothNet [90] is used to smooth the SMPL-T parameters after 2D keypoint based optimization. We evaluate this step by computing the SMPL errors, shown in Tab. 4. We can see that SmoothNet reduces the SMPL error slightly.

Method	Chamfer	v2v	Acceleration
w/o SmoothNet	8.71	9.84	1.38
w/ SmoothNet	**8.01**	**9.12**	**1.18**

Table 4. Ablate SMPL SmoothNet (errors in cm). We can see that SmoothNet [90] improves the overall smoothness and slightly reduces the pose errors.

Method	Chamfer	v2v	Translation
a. Raw prediction	5.03	10.39	10.01
b. Raw + SmoothNet	4.22	8.60	10.16
c. Raw + our pose pred.	4.09	8.02	10.20
d. Our full model	**3.62**	**7.20**	**9.96**

Table 5. Ablate SmoothNet for object pose prediction (errors in cm). We can see our pose prediction (c) is better than Smooth-Net [90] (b). Combing both we obtain the best result (d).

We also use SmoothNet to smooth the object pose before sending it to our human and visibility aware object pose prediction network. SmoothNet cannot correct errors under long-term occlusions. However, it provides smoother object motion for visible frames which can benefit our pose prediction network. We evaluate this using object pose errors and report the results in Tab. 5. It can be seen that our method (Tab. 5c) works better than SmoothNet (Tab. 5b) on raw predictions. Nevertheless, with smoothed pose after SmoothNet, our method achieves the best result (Tab. 5 d).

B.4. Runtime cost

SMPL-T pre-fitting and joint optimization can be run in batches hence the average runtime per frame is not long: SMPL-T pre-fitting: 6.38s, SIF-Net object pose prediction: 0.89s, HVOP-Net: 1.3ms, joint optimization: 9.26s, total: 16.53s. Compared to CHORE (∼12s/frame) [80], the additional cost is mainly from the SMPL-T pre-fitting. Yet, SMPL-T conditioning allows faster convergence of joint optimization and much better reconstruction. Since we use efficient 2D encoder instead of 3D encoder, it takes only 1.05GB GPU memory to load the SIF-Net model. This allows us to do joint optimization with batch size up to 128 on a GPU with 48GB memory.

Appendix C. Generalization to NTU-RGBD dataset

Obtaining input masks. Unlike BEHAVE and InterCap where the human and object masks are provided by the dataset, there are no masks in NTU-RGBD. To this end, we run DetectronV2 [79] to obtain the human masks. We manually segment the object in the first frame using interactive segmentation [64] (<1min/image) and then use video segmentation [14] to propagate the masks. The overhead of 1min/video manual label is small.

We show more results from our method on NTU-RGBD dataset [47] and compare against CHORE [80] in Fig. 11.

A. Significant object pose change between two visible frames.
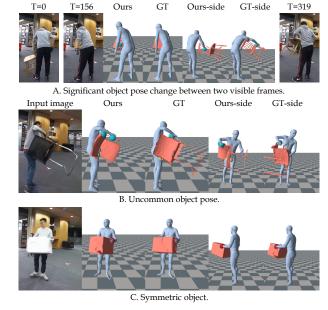

B. Uncommon object pose.

C. Symmetric object.

Figure 9. Failure cases analysis. We show three typical failure cases of our method: A. The occluded object pose (T=156) changes significantly between two visible frames (T=0 and T=319) and it is difficult to accurate track the contact changes. B. The object pose is not commonly seen during interaction and it is difficult to predict for this rare pose. C. The object is symmetric. The joint optimization satisfies the object mask and contacts but is not semantically correct.

It can be seen that CHORE may predict some reasonable object pose but it fails quite often to capture the fine-grained contacts between the human and object. Our method obtains more coherent reconstruction for different subjects, human-backpack interactions, camera view points and backgrounds. Please see our project website for comparison in full sequences.

Appendix D. Limitations and future works

Although our method works robustly under heavy occlusions, there are still some limitations. Firstly, we assume known object templates for tracking, an interesting direction is to build such a template from videos as demonstrated by recent works [78,82–84]. Secondly, it would be interesting to model multi-person or even multi-object interactions which is a more realistic setting in real-life applications. In addition, the backpack can also deform non-rigidly which is not modelled in our method. Further works can incorporate the surface deformation [46] or object articulation [81] into the human object interaction. We leave these for future works.

We identify three typical failure cases of our method, some examples are shown in Fig. 9. The first typical failure case comes from heavy occlusion when the object undergoes significant changes (object pose and contact locations)

between two visible frames. In this case, it is very difficult to track the pose and contact changes accurately (Fig. 9 A). Second typical failure is due to the difficulty of pose prediction itself even the object is fully visible. In this case the object pose is uncommon and the network failed to predict it correctly (Fig. 9 B). Another failure is caused by symmetric objects. Our optimization minimizes the 2D mask loss and contact constraints but the network is confused by the symmetry and the initial pose prediction is not semantically correct (Fig. 9 C). In addition, the training data for these objects is very limited (only $1/3$ of other objects). More training data or explicitly reasoning about the symmetry [94] can be helpful.

References

[1] http://virtualhumans.mpi-inf.mpg.de/people.html. 8

[2] Thiemo Alldieck, Marcus Magnor, Weipeng Xu, Christian Theobalt, and Gerard Pons-Moll. Detailed human avatars from monocular video. In *International Conf. on 3D Vision*, sep 2018. 2

[3] Thiemo Alldieck, Marcus Magnor, Weipeng Xu, Christian Theobalt, and Gerard Pons-Moll. Video based reconstruction of 3D people models. In *IEEE Conf. on Computer Vision and Pattern Recognition*, 2018. 2

[4] Bharat Lal Bhatnagar, Cristian Sminchisescu, Christian Theobalt, and Gerard Pons-Moll. Combining implicit function learning and parametric models for 3d human reconstruction. In *European Conference on Computer Vision (ECCV)*. Springer, August 2020. 2, 4, 5

[5] Bharat Lal Bhatnagar, Cristian Sminchisescu, Christian Theobalt, and Gerard Pons-Moll. Loopreg: Self-supervised learning of implicit surface correspondences, pose and shape for 3d human mesh registration. In *Advances in Neural Information Processing Systems (NeurIPS)*, December 2020. 2

[6] Bharat Lal Bhatnagar, Xianghui Xie, Ilya Petrov, Cristian Sminchisescu, Christian Theobalt, and Gerard Pons-Moll. Behave: Dataset and method for tracking human object interactions. In *IEEE Conference on Computer Vision and Pattern Recognition (CVPR)*, June 2022. 1, 2, 3, 6, 7, 10

[7] Federica Bogo, Angjoo Kanazawa, Christoph Lassner, Peter Gehler, Javier Romero, and Michael J Black. Keep it SMPL: Automatic estimation of 3D human pose and shape from a single image. In *European Conf. on Computer Vision*. Springer International Publishing, 2016. 2, 3

[8] Derek Bradley, Tiberiu Popa, Alla Sheffer, Wolfgang Heidrich, and Tamy Boubekeur. Markerless garment capture. *ACM Trans. Graph.*, 27(3):1–9, aug 2008. 1

[9] Samarth Brahmbhatt, Cusuh Ham, Charles C. Kemp, and James Hays. ContactDB: Analyzing and predicting grasp contact via thermal imaging. In *The IEEE Conference on Computer Vision and Pattern Recognition (CVPR)*, 2019. 2

[10] Samarth Brahmbhatt, Ankur Handa, James Hays, and Dieter Fox. Contactgrasp: Functional multi-finger grasp synthesis from contact. In *IROS*, 04 2019. 2

[11] Samarth Brahmbhatt, Chengcheng Tang, Christopher D. Twigg, Charles C. Kemp, and James Hays. ContactPose: A dataset of grasps with object contact and hand pose. In *The European Conference on Computer Vision (ECCV)*, August 2020. 2

[12] Z. Cao, G. Hidalgo Martinez, T. Simon, S. Wei, and Y. A. Sheikh. Openpose: Realtime multi-person 2d pose estimation using part affinity fields. *IEEE Transactions on Pattern Analysis and Machine Intelligence*, 2019. 3

[13] Eric R. Chan, Connor Z. Lin, Matthew A. Chan, Koki Nagano, Boxiao Pan, Shalini De Mello, Orazio Gallo, Leonidas Guibas, Jonathan Tremblay, Sameh Khamis, Tero Karras, and Gordon Wetzstein. Efficient geometry-aware 3D generative adversarial networks. In *CVPR*, 2022. 4

[14] Ho Kei Cheng, Yu-Wing Tai, and Chi-Keung Tang. Modular interactive video object segmentation: Interaction-to-mask, propagation and difference-aware fusion. In *CVPR*, 2021. 8, 11

[15] Julian Chibane, Thiemo Alldieck, and Gerard Pons-Moll. Implicit functions in feature space for 3d shape reconstruction and completion. In *IEEE Conference on Computer Vision and Pattern Recognition (CVPR)*. IEEE, jun 2020. 4

[16] Julian Chibane, Aymen Mir, and Gerard Pons-Moll. Neural unsigned distance fields for implicit function learning. In *Neural Information Processing Systems (NeurIPS)*. , December 2020. 4, 5

[17] Alvaro Collet, Ming Chuang, Pat Sweeney, Don Gillett, Dennis Evseev, David Calabrese, Hugues Hoppe, Adam Kirk, and Steve Sullivan. High-quality streamable free-viewpoint video. *ACM Trans. Graph.*, 34(4), jul 2015. 1

[18] Enric Corona, Gerard Pons-Moll, Guillem Alenya, and Francesc Moreno-Noguer. Learned vertex descent: A new direction for 3d human model fitting. In *European Conference on Computer Vision (ECCV)*. Springer, October 2022. 2

[19] Enric Corona, Albert Pumarola, Guillem Alenya, Francesc Moreno-Noguer, and Gregory Rogez. Ganhand: Predicting human grasp affordances in multi-object scenes. In *Proceedings of the IEEE/CVF Conference on Computer Vision and Pattern Recognition (CVPR)*, June 2020. 2

[20] Yudi Dai, YiTai Lin, XiPing Lin, Chenglu Wen, Lan Xu, Hongwei Yi, Siqi Shen, Yuexin Ma, and Cheng Wang. Sloper4d: A scene-aware dataset for global 4d human pose estimation in urban environments. In *IEEE Conference on Computer Vision and Pattern Recognition (CVPR)*, June 2023. 2

[21] Xinke Deng, Arsalan Mousavian, Yu Xiang, Fei Xia, Timothy Bretl, and Dieter Fox. PoseRBPF: A Rao–Blackwellized Particle Filter for 6-D Object Pose Tracking. *IEEE Transactions on Robotics*, 37(5):1328–1342, Oct. 2021. Conference Name: IEEE Transactions on Robotics. 2

[22] Yan Di, Fabian Manhardt, Gu Wang, Xiangyang Ji, Nassir Navab, and Federico Tombari. SO-Pose: Exploiting Self-Occlusion for Direct 6D Pose Estimation. In *2021 IEEE/CVF International Conference on Computer Vision (ICCV)*, pages 12376–12385, Montreal, QC, Canada, Oct. 2021. IEEE. 2

[23] Yinglin Duan, Yue Lin, Zhengxia Zou, Yi Yuan, Zhehui Qian, and Bohan Zhang. A unified framework for real time

motion completion. *Proceedings of the AAAI Conference on Artificial Intelligence*, 36(4):4459–4467, Jun. 2022. 5

[24] Kiana Ehsani, Shubham Tulsiani, Saurabh Gupta, Ali Farhadi, and Abhinav Gupta. Use the force, luke! learning to predict physical forces by simulating effects. In *CVPR*, 2020. 2

[25] Zhaoxin Fan, Yazhi Zhu, Yulin He, Qi Sun, Hongyan Liu, and Jun He. Deep Learning on Monocular Object Pose Detection and Tracking: A Comprehensive Overview, Apr. 2022. arXiv:2105.14291 [cs]. 2

[26] Mihai Fieraru, Mihai Zanfir, Elisabeta Oneata, Alin-Ionut Popa, Vlad Olaru, and Cristian Sminchisescu. Three-dimensional reconstruction of human interactions. In *2020 IEEE/CVF Conference on Computer Vision and Pattern Recognition (CVPR)*, pages 7212–7221, 2020. 2

[27] Vladimir Guzov, Aymen Mir, Torsten Sattler, and Gerard Pons-Moll. Human poseitioning system (hps): 3d human pose estimation and self-localization in large scenes from body-mounted sensors. In *IEEE Conference on Computer Vision and Pattern Recognition (CVPR)*. IEEE, jun 2021. 2

[28] Shreyas Hampali, Mahdi Rad, Markus Oberweger, and Vincent Lepetit. Honnotate: A method for 3d annotation of hand and object poses. In *CVPR*, 2020. 2

[29] Mohamed Hassan, Vasileios Choutas, Dimitrios Tzionas, and Michael J. Black. Resolving 3d human pose ambiguities with 3d scene constraints. In *International Conference on Computer Vision*, 2019. 2

[30] Yana Hasson, Gül Varol, Dimitrios Tzionas, Igor Kalevatykh, Michael J. Black, Ivan Laptev, and Cordelia Schmid. Learning joint reconstruction of hands and manipulated objects. In *CVPR*, 2019. 2

[31] Sachini Herath, Hang Yan, and Yasutaka Furukawa. Ronin: Robust neural inertial navigation in the wild: Benchmark, evaluations, new methods. In *2020 IEEE International Conference on Robotics and Automation (ICRA)*, pages 3146–3152, 2020. 6

[32] Tomáš Hodaň, Jiří Matas, and Štěpán Obdržálek. On evaluation of 6d object pose estimation. In Gang Hua and Hervé Jégou, editors, *Computer Vision – ECCV 2016 Workshops*, pages 606–619, Cham, 2016. Springer International Publishing. 6

[33] Yinlin Hu, Pascal Fua, Wei Wang, and Mathieu Salzmann. Single-stage 6d object pose estimation. In *CVPR*, 2020. 2

[34] Chun-Hao P. Huang, Hongwei Yi, Markus Höschle, Matvey Safroshkin, Tsvetelina Alexiadis, Senya Polikovsky, Daniel Scharstein, and Michael J. Black. Capturing and inferring dense full-body human-scene contact. In *IEEE/CVF Conf. on Computer Vision and Pattern Recognition (CVPR)*, pages 13274–13285, June 2022. 1, 2

[35] Yinghao Huang, Omid Taheri, Michael J. Black, and Dimitrios Tzionas. InterCap: Joint markerless 3D tracking of humans and objects in interaction. In *German Conference on Pattern Recognition (GCPR)*, volume 13485 of *Lecture Notes in Computer Science*, pages 281–299. Springer, 2022. 2, 3, 6, 7, 10

[36] Yuheng Jiang, Suyi Jiang, Guoxing Sun, Zhuo Su, Kaiwen Guo, Minye Wu, Jingyi Yu, and Lan Xu. Neuralho-

[37] Hanbyul Joo, Tomas Simon, and Yaser Sheikh. Total capture: A 3d deformation model for tracking faces, hands, and bodies. In *2018 IEEE/CVF Conference on Computer Vision and Pattern Recognition*, pages 8320–8329, 2018. 1

[38] Korrawe Karunratanakul, Jinlong Yang, Yan Zhang, Michael Black, Krikamol Muandet, and Siyu Tang. Grasping field: Learning implicit representations for human grasps. In *8th International Conference on 3D Vision*, pages 333–344. IEEE, Nov. 2020. 2

[39] Jihoon Kim, Taehyun Byun, Seungyoun Shin, Jungdam Won, and Sungjoon Choi. Conditional motion in-betweening. *Pattern Recognition*, page 108894, 2022. 5, 6, 8, 10, 16

[40] Muhammed Kocabas, Nikos Athanasiou, and Michael J. Black. Vibe: Video inference for human body pose and shape estimation. In *The IEEE Conference on Computer Vision and Pattern Recognition (CVPR)*, June 2020. 2

[41] Muhammed Kocabas, Chun-Hao P. Huang, Otmar Hilliges, and Michael J. Black. PARE: Part attention regressor for 3D human body estimation. In *Proceedings International Conference on Computer Vision (ICCV)*, pages 11127–11137. IEEE, Oct. 2021. 2

[42] Muhammed Kocabas, Chun-Hao P. Huang, Joachim Tesch, Lea Müller, Otmar Hilliges, and Michael J. Black. SPEC: Seeing people in the wild with an estimated camera. In *Proceedings International Conference on Computer Vision (ICCV)*, pages 11035–11045. IEEE, Oct. 2021. 2, 6

[43] Nikos Kolotouros, Georgios Pavlakos, Michael J Black, and Kostas Daniilidis. Learning to reconstruct 3d human pose and shape via model-fitting in the loop. In *ICCV*, 2019. 2

[44] Jake Levinson, Carlos Esteves, Kefan Chen, Noah Snavely, Angjoo Kanazawa, Afshin Rostamizadeh, and Ameesh Makadia. An analysis of svd for deep rotation estimation. In H. Larochelle, M. Ranzato, R. Hadsell, M.F. Balcan, and H. Lin, editors, *Advances in Neural Information Processing Systems*, volume 33, pages 22554–22565. Curran Associates, Inc., 2020. 4

[45] Yi Li, Gu Wang, Xiangyang Ji, Yu Xiang, and Dieter Fox. Deepim: Deep iterative matching for 6d pose estimation. In *European Conference on Computer Vision (ECCV)*, 2018. 2

[46] Zhi Li, Soshi Shimada, Bernt Schiele, Christian Theobalt, and Vladislav Golyanik. Mocapdeform: Monocular 3d human motion capture in deformable scenes. In *International Conference on 3D Vision (3DV)*, 2022. 2, 11

[47] Jun Liu, Amir Shahroudy, Mauricio Perez, Gang Wang, Ling-Yu Duan, and Alex C. Kot. Ntu rgb+d 120: A large-scale benchmark for 3d human activity understanding. *IEEE Transactions on Pattern Analysis and Machine Intelligence*, 2019. 8, 9, 11, 17

[48] Yuan Liu, Yilin Wen, Sida Peng, Cheng Lin, Xiaoxiao Long, Taku Komura, and Wenping Wang. Gen6d: Generalizable model-free 6-dof object pose estimation from rgb images. In *ECCV*, 2022. 2

[49] Matthew Loper, Naureen Mahmood, Javier Romero, Gerard Pons-Moll, and Michael J. Black. SMPL: A skinned multi-

person linear model. In *ACM Transactions on Graphics*. ACM, Oct. 2015. 2, 3, 5

[50] Mateusz Majcher and Bogdan Kwolek. Shape enhanced keypoints learning with geometric prior for 6d object pose tracking. In *2022 IEEE/CVF Conference on Computer Vision and Pattern Recognition Workshops (CVPRW)*, pages 2985–2991, 2022. 2

[51] Alejandro Newell, Kaiyu Yang, and Jia Deng. Stacked hourglass networks for human pose estimation. In Bastian Leibe, Jiri Matas, Nicu Sebe, and Max Welling, editors, *Computer Vision – ECCV 2016*, pages 483–499, Cham, 2016. Springer International Publishing. 9

[52] Georgios Pavlakos, Vasileios Choutas, Nima Ghorbani, Timo Bolkart, Ahmed A. A. Osman, Dimitrios Tzionas, and Michael J. Black. Expressive body capture: 3d hands, face, and body from a single image. In *Proceedings IEEE Conf. on Computer Vision and Pattern Recognition (CVPR)*, 2019. 2, 3

[53] Sida Peng, Yuan Liu, Qixing Huang, Xiaowei Zhou, and Hujun Bao. PVNet: Pixel-Wise Voting Network for 6DoF Pose Estimation. In *2019 IEEE/CVF Conference on Computer Vision and Pattern Recognition (CVPR)*, pages 4556–4565, Long Beach, CA, USA, June 2019. IEEE. 2

[54] Ilya A Petrov, Riccardo Marin, Julian Chibane, and Gerard Pons-Moll. Object pop-up: Can we infer 3d objects and their poses from human interactions alone? In *Proceedings of the IEEE/CVF Conference on Computer Vision and Pattern Recognition*, 2023. 2

[55] Gerard Pons-Moll and Bodo Rosenhahn. *Model-Based Pose Estimation*, chapter 9, pages 139–170. Springer, 2011. 2

[56] Jathushan Rajasegaran, Georgios Pavlakos, Angjoo Kanazawa, and Jitendra Malik. Tracking people with 3d representations. *Advances in Neural Information Processing Systems*, 34:23703–23713, 2021. 2

[57] Jathushan Rajasegaran, Georgios Pavlakos, Angjoo Kanazawa, and Jitendra Malik. Tracking people by predicting 3d appearance, location and pose. In *Proceedings of the IEEE/CVF Conference on Computer Vision and Pattern Recognition*, pages 2740–2749, 2022. 2

[58] Davis Rempe, Tolga Birdal, Aaron Hertzmann, Jimei Yang, Srinath Sridhar, and Leonidas J. Guibas. Humor: 3d human motion model for robust pose estimation. In *International Conference on Computer Vision (ICCV)*, 2021. 2

[59] Chris Rockwell and David F. Fouhey. Full-body awareness from partial observations. In *ECCV*, 2020. 2

[60] Yu Rong, Takaaki Shiratori, and Hanbyul Joo. Frankmocap: A monocular 3d whole-body pose estimation system via regression and integration. In *IEEE International Conference on Computer Vision Workshops*, 2021. 3

[61] Shunsuke Saito, , Zeng Huang, Ryota Natsume, Shigeo Morishima, Angjoo Kanazawa, and Hao Li. Pifu: Pixel-aligned implicit function for high-resolution clothed human digitization. In *IEEE International Conference on Computer Vision (ICCV)*. IEEE, oct 2019. 2, 4

[62] Shunsuke Saito, Tomas Simon, Jason Saragih, and Hanbyul Joo. Pifuhd: Multi-level pixel-aligned implicit function for high-resolution 3d human digitization. In *Proceedings of the*

IEEE Conference on Computer Vision and Pattern Recognition*, June 2020. 4

[63] Soshi Shimada, Vladislav Golyanik, Zhi Li, Patrick Pérez, Weipeng Xu, and Christian Theobalt. Hulc: 3d human motion capture with pose manifold sampling and dense contact guidance. In *European Conference on Computer Vision (ECCV)*, pages 516–533, 2022. 2

[64] Konstantin Sofiiuk, Ilia Petrov, Olga Barinova, and Anton Konushin. f-brs: Rethinking backpropagating refinement for interactive segmentation. In *Proceedings of the IEEE/CVF Conference on Computer Vision and Pattern Recognition*, pages 8623–8632, 2020. 8, 11

[65] Manuel Stoiber, Martin Sundermeyer, and Rudolph Triebel. Iterative Corresponding Geometry: Fusing Region and Depth for Highly Efficient 3D Tracking of Textureless Objects. In *2022 IEEE/CVF Conference on Computer Vision and Pattern Recognition (CVPR)*, pages 6845–6855, New Orleans, LA, USA, June 2022. IEEE. 2

[66] Jürgen Sturm, Stéphane Magnenat, Nikolas Engelhard, François Pomerleau, Francis Colas, Daniel Cremers, Roland Siegwart, and Wolfram Burgard. Towards a benchmark for RGB-D SLAM evaluation. In *RGB-D Workshop on Advanced Reasoning with Depth Cameras at Robotics: Science and Systems Conf.(RSS)*, Los Angeles, United States, 2011. 6

[67] Guoxing Sun, Xin Chen, Yizhang Chen, Anqi Pang, Pei Lin, Yuheng Jiang, Lan Xu, Jingya Wang, and Jingyi Yu. Neural free-viewpoint performance rendering under complex human-object interactions. In *Proceedings of the 29th ACM International Conference on Multimedia*, 2021. 2

[68] Jiaming Sun, Zihao Wang, Siyu Zhang, Xingyi He, Hongcheng Zhao, Guofeng Zhang, and Xiaowei Zhou. OnePose: One-shot object pose estimation without CAD models. *CVPR*, 2022. 2

[69] Omid Taheri, Nima Ghorbani, Michael J. Black, and Dimitrios Tzionas. GRAB: A dataset of whole-body human grasping of objects. In *European Conference on Computer Vision (ECCV)*, 2020. 2, 3

[70] Yating Tian, Hongwen Zhang, Yebin Liu, and Limin Wang. Recovering 3d human mesh from monocular images: A survey. *arXiv preprint arXiv:2203.01923*, 2022. 2

[71] Garvita Tiwari, Dimitrije Antic, Jan Eric Lenssen, Nikolaos Sarafianos, Tony Tung, and Gerard Pons-Moll. Posendf: Modeling human pose manifolds with neural distance fields. In *European Conference on Computer Vision (ECCV)*. Springer, October 2022. 3

[72] Ashish Vaswani, Noam Shazeer, Niki Parmar, Jakob Uszkoreit, Llion Jones, Aidan N Gomez, Ł ukasz Kaiser, and Illia Polosukhin. Attention is all you need. In I. Guyon, U. Von Luxburg, S. Bengio, H. Wallach, R. Fergus, S. Vishwanathan, and R. Garnett, editors, *Advances in Neural Information Processing Systems*, volume 30. Curran Associates, Inc., 2017. 5, 9

[73] Gu Wang, Fabian Manhardt, Federico Tombari, and Xiangyang Ji. GDR-Net: Geometry-guided direct regression network for monocular 6d object pose estimation. In *IEEE/CVF Conference on Computer Vision and Pattern Recognition (CVPR)*, pages 16611–16621, June 2021. 2

[74] Xi Wang, Gen Li, Yen-Ling Kuo, Muhammed Kocabas, Emre Aksan, and Otmar Hilliges. Reconstructing action-conditioned human-object interactions using commonsense knowledge priors. In *International Conference on 3D Vision (3DV)*, 2022. 2

[75] Bowen Wen and Kostas Bekris. BundleTrack: 6D Pose Tracking for Novel Objects without Instance or Category-Level 3D Models. In *2021 IEEE/RSJ International Conference on Intelligent Robots and Systems (IROS)*, pages 8067–8074, Prague, Czech Republic, Sept. 2021. IEEE Press. 2

[76] Bowen Wen, Chaitanya Mitash, Baozhang Ren, and Kostas E. Bekris. se(3)-tracknet: Data-driven 6d pose tracking by calibrating image residuals in synthetic domains. *2020 IEEE/RSJ International Conference on Intelligent Robots and Systems (IROS)*, Oct 2020. 2

[77] Zhenzhen Weng and Serena Yeung. Holistic 3d human and scene mesh estimation from single view images. *arXiv preprint arXiv:2012.01591*, 2020. 2

[78] Shangzhe Wu, Tomas Jakab, Christian Rupprecht, and Andrea Vedaldi. DOVE: Learning deformable 3d objects by watching videos. *arXiv preprint arXiv:2107.10844*, 2021. 8, 11

[79] Yuxin Wu, Alexander Kirillov, Francisco Massa, Wan-Yen Lo, and Ross Girshick. Detectron2. https://github.com/facebookresearch/detectron2, 2019. 8, 11

[80] Xianghui Xie, Bharat Lal Bhatnagar, and Gerard Pons-Moll. Chore: Contact, human and object reconstruction from a single rgb image. In *European Conference on Computer Vision (ECCV)*. Springer, October 2022. 1, 2, 3, 4, 5, 6, 7, 8, 9, 11, 17

[81] Xiang Xu, Hanbyul Joo, Greg Mori, and Manolis Savva. D3d-hoi: Dynamic 3d human-object interactions from videos. *arXiv preprint arXiv:2108.08420*, 2021. 11

[82] Gengshan Yang, Deqing Sun, Varun Jampani, Daniel Vlasic, Forrester Cole, Huiwen Chang, Deva Ramanan, William T Freeman, and Ce Liu. Lasr: Learning articulated shape reconstruction from a monocular video. In *CVPR*, 2021. 8, 11

[83] Gengshan Yang, Deqing Sun, Varun Jampani, Daniel Vlasic, Forrester Cole, Ce Liu, and Deva Ramanan. Viser: Video-specific surface embeddings for articulated 3d shape reconstruction. In *NeurIPS*, 2021. 8, 11

[84] Gengshan Yang, Minh Vo, Natalia Neverova, Deva Ramanan, Andrea Vedaldi, and Hanbyul Joo. Banmo: Building animatable 3d neural models from many casual videos. In *CVPR*, 2022. 8, 11

[85] Lixin Yang, Xinyu Zhan, Kailin Li, Wenqiang Xu, Jiefeng Li, and Cewu Lu. CPF: Learning a contact potential field to model the hand-object interaction. In *ICCV*, 2021. 2, 3

[86] Hongwei Yi, Chun-Hao P. Huang, Shashank Tripathi, Lea Hering, Justus Thies, and Michael J. Black. MIME: Human-aware 3D scene generation. In *IEEE Conference on Computer Vision and Pattern Recognition (CVPR)*, June 2023. 2

[87] Hongwei Yi, Chun-Hao P. Huang, Dimitrios Tzionas, Muhammed Kocabas, Mohamed Hassan, Siyu Tang, Justus Thies, and Michael J. Black. Human-aware object placement for visual environment reconstruction. In *IEEE/CVF*

Conf. on Computer Vision and Pattern Recognition (CVPR), pages 3959–3970, June 2022. 2

[88] Hongwei Yi, Hualin Liang, Yifei Liu, Qiong Cao, Yandong Wen, Timo Bolkart, Dacheng Tao, and Michael J Black. Generating holistic 3d human motion from speech. In *IEEE Conference on Computer Vision and Pattern Recognition (CVPR)*, June 2023. 5

[89] Ye Yuan, Umar Iqbal, Pavlo Molchanov, Kris Kitani, and Jan Kautz. Glamr: Global occlusion-aware human mesh recovery with dynamic cameras. In *Proceedings of the IEEE/CVF Conference on Computer Vision and Pattern Recognition (CVPR)*, 2022. 2, 5, 6

[90] Ailing Zeng, Lei Yang, Xuan Ju, Jiefeng Li, Jianyi Wang, and Qiang Xu. Smoothnet: A plug-and-play network for refining human poses in videos. In *European Conference on Computer Vision*. Springer, 2022. 4, 5, 6, 8, 10, 11

[91] Jason Y. Zhang, Sam Pepose, Hanbyul Joo, Deva Ramanan, Jitendra Malik, and Angjoo Kanazawa. Perceiving 3d human-object spatial arrangements from a single image in the wild. In *European Conference on Computer Vision (ECCV)*, 2020. 1, 2, 5, 6, 7

[92] Tianshu Zhang, Buzhen Huang, and Yangang Wang. Object-occluded human shape and pose estimation from a single color image. In *2020 IEEE/CVF Conference on Computer Vision and Pattern Recognition (CVPR)*, pages 7374–7383, 2020. 2

[93] Xiaohan Zhang, Bharat Lal Bhatnagar, Sebastian Starke, Vladimir Guzov, and Gerard Pons-Moll. Couch: Towards controllable human-chair interactions. In *European Conference on Computer Vision (ECCV)*. Springer, October 2022. 2, 5

[94] Linfang Zheng, Aleš Leonardis, Tze Ho Elden Tse, Nora Horanyi, Hua Chen, Wei Zhang, and Hyung Jin Chang. TP-AE: Temporally Primed 6D Object Pose Tracking with Auto-Encoders. In *2022 International Conference on Robotics and Automation (ICRA)*, pages 10616–10623, Philadelphia, PA, USA, May 2022. IEEE Press. 2, 12

[95] Keyang Zhou, Bharat Lal Bhatnagar, Jan Eric Lenssen, and Gerard Pons-Moll. Toch: Spatio-temporal object correspondence to hand for motion refinement. In *European Conference on Computer Vision (ECCV)*. Springer, October 2022. 2, 3

[96] Yi Zhou, Connelly Barnes, Lu Jingwan, Yang Jimei, and Li Hao. On the continuity of rotation representations in neural networks. In *The IEEE Conference on Computer Vision and Pattern Recognition (CVPR)*, June 2019. 9
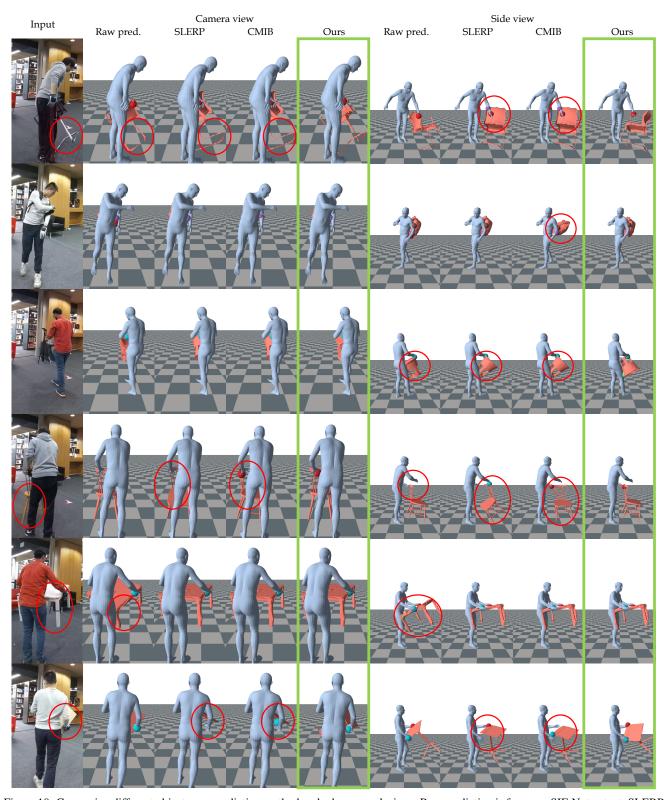
Figure 10. Comparing different object pose prediction method under heavy occlusions. Raw prediction is from our SIF-Net output, SLERP denotes linear interpolation and CMIB is from [39]. We can see SLERP and CMIB can correct some errors (row 5) but they do not take the human motion into account hence often fail in more challenging cases. Our method is more robust as it leverages information from both human motion and object pose from visible frames.
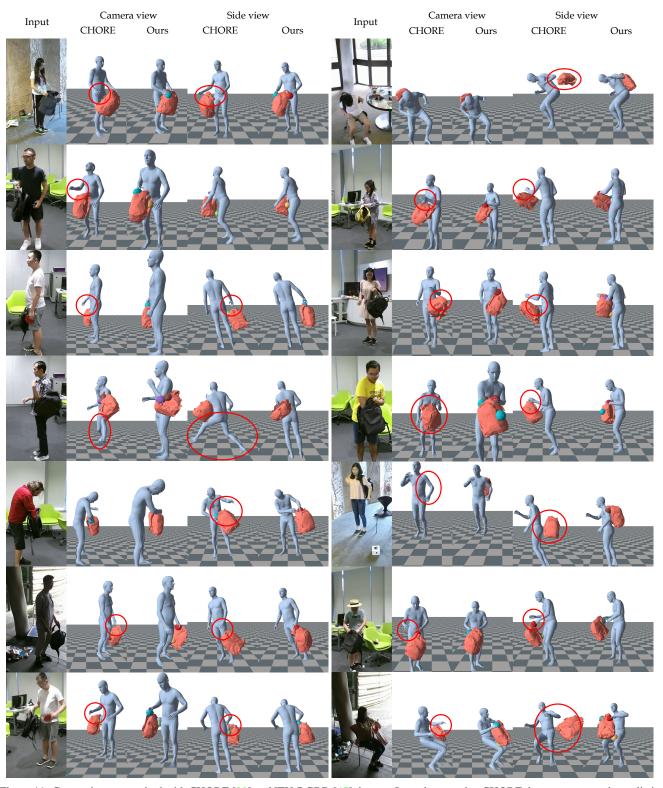
Figure 11. Comparing our method with CHORE [80] on NTU-RGBD [47] dataset. It can be seen that CHORE does not capture the realistic contacts between the person and the backpack. Our method recovers the 3D human, the object and contacts more faithfully in different interaction types, camera view points and backgrounds.